Design and Control of the Lift Subsystem of a Two-Wheeled Forklift Robot

1st Sergio Esteban Quintero Benavides
Graduate School of Integrated Design Engineering
Keio University
Yokohama, Japan
sergio@sum.sd.keio.ac.jp

2nd Toshiyuki Murakami
Department of System Design Engineering
Keio University
Yokohama, Japan
mura@sd.keio.ac.jp

***Abstract*—This paper proposes the mechanical design and control of the lift subsystem of a Two-Wheeled Forklift Robot (TWFR). Vertical movement is achieved by employing a ball screw linear actuator that creates a movement of the fork relative to the main body of the robot. Vertical stabilization and trajectory generation of the robot are achieved by implementing a precise positioning of the Center of Gravity (CoG) of the complete system; this positioning considers the dynamic effects of changing the height of the load by the implementation of Reaction Torque Observers (RTOBs) and a special Inverse Kinematics (IK) solution that takes into account not only the position of the end effector but also the coordinates of the CoG. The low-level strategies for controlling pitch angle, fork angle, and lift height implement different disturbance observers and PD controllers to move the end effector and CoG to the desired position relative to the main axis of the wheels, allowing also a precise generation of the system trajectory. The performance of the trajectory generation and control strategies is tested in simulation to validate the proposed architecture.**

***Index Terms*—Two-Wheeled Forklift Robot (TWFR), Mechanical design, Disturbance observer, Model-based control, CoG positioning, Motion planning.**

I. Introduction

In modern industrial environments, humans and robots must work together ”side by side”. In several countries, there is a labor shortage due to the low birth rate that has been observed around the world in the last decades, creating, as a consequence, aging societies. In addition, robotic systems are employed to carry out tasks that involve health risks to human workers. In warehouses or assembly lines, the movement of load or material is a main task, which, executed repetitively by humans, could lead to future chronic physical problems. However, implementing mobile robotic systems must also guarantee the safety of the workspace. Considering these factors, a Two-Wheeled Forklift Robot (TWFR) is proposed to optimize the space occupied by the robot and reduce the impact force during a potential collision due to its compact design.

This work aims to propose the mechanical design and control of the lift subsystem of a TWFR. The mechanical design of the lift focuses on a modular approach that offers flexibility for the distribution of mass inside the main body of the robot. For that reason, a ball screw linear actuator is proposed for the vertical movement of the fork; this particular mechanism offers high accuracy, repeatability and maximum payload, important features for this particular application.

The system's control is achieved by the implementation of different disturbance observers and PD controllers in the different subsystems of the robot. Works such as [1], [2], and [3] use the Synthesized Pitch Angle Disturbance Observer (SPADO) to model the unified disturbances that affect the wheels' angle and the robot's pitch angle. It is important to have this synthesized disturbance observer because of the underactuated condition of the system.

The dynamics of Two-Wheeled Robots (TWR) depend on the position of their Center of Gravity (CoG); thus, the position of the CoG not only stabilizes the system but also drives its trajectory, for that reason, the position of the end effector and the CoG should be considered in an unified Inverse Kinematics (IK) solution, common in loco-manipulation platforms. This particular solution must also take into account the effects of the external load on the position of the CoG, which is why different Reaction Torque Observers (RTOBs) are used to estimate the external load placed over the fork and change the reference CoG position accordingly. The controller for the rotational joint of the fork uses a disturbance observer to compensate for the effects of the external load and the internal residual torques. The position control of the fork is done by a PD controller that makes sure the fork is parallel to the ground when the external load is placed on it.

The same previously discussed control architecture for the lift subsystem is proposed. A disturbance observer is used to compensate for the external and internal forces that affect the mechanism, and a PD controller regulates the linear movement of the lift to move the load vertically to the desired height. The experiments confirmed the capability of the system to achieve the desired vertical movement of the load and the possibility of estimating the weight of the external load by implementing a RTOB that considers only the linear movement of the lift.

This work aims to propose the mechanical design and control for the lift subsystem of an existing TWFR. The design of the lift is discussed in section II, the mathematical model of the robot including the new linear subsystem and the effects of the position of the CoG on the trajectory of the robot is presented in section III, the control of the robot is discussed in section IV where a PD controller and

a disturbance observer is proposed to control the vertical displacement of the lift, furthermore, it presents how RTOB implemented on the fork and lift sysbsystems are used to estimate the weight and position of the external load over the fork. Section V presents the simulation results of the proposed controller in a simple motion task that demonstrates the performance of the integrated system. Finally, this paper presents in section VI the conclusions of the presented paper and the future work.

II. Mechanical design

The physical implementation of the TWFR requires a linear actuator that lifts the base plate where the fork mechanism is assembled. The current work propose the implementation of a ball screw linear actuator with a stroke of 350mm, maximum vertical payload of 40kg, maximum linear speed of 300mm/s, and maximum acceleration of 0.15g. Considering a maximum external load of 10kg and contemplating that the desired application motion profiles do not exceed the velocity and acceleration limits, the selected actuator is a feasible option. Fig. 1 represents the design of the TWFR with the proposed vertical linear actuator.

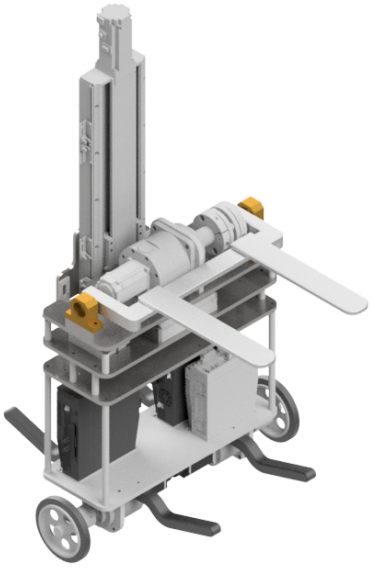

Fig. 1: Design of the TWFR.

III. Modeling

This section describes the mathematical modeling of the TWFR using the scheme presented in Fig. 2 and the parameters described in Table I as reference. Taking into account that the main function of the robot is to move the load that is placed over the fork, the orientation of the end effector must remain as constant as possible, parallel to the floor. This condition implies that $\theta_p + \theta_a = 0$ for the system's steady state; this expression will be used throughout this section to simplify the presented equations.

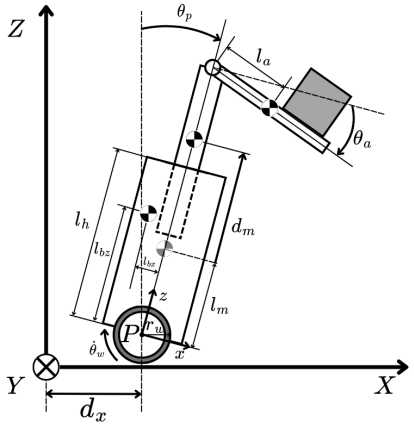

Fig. 2: Abstraction model of the TWFR.

Table I: Model parameters of the TWFR

Parameter	Explanation
θ_w	Wheels angle
θ_p	Pitch angle
d_m	Lift displacement
θ_a	Arm angle
$\mathrm{l_{bx}}$	Body CoG x coordinate
$\mathrm{l_{bz}}$	Body CoG z coordinate
$\mathrm{l_m}$	Lift CoG distance
$\mathrm{l_h}$	Body length
$\mathrm{l_a}$	Arm CoG distance
$\mathrm{m_b}$	Body mass
$\mathrm{m_m}$	Lift mass
$\mathrm{m_a}$	Arm mass
$\mathrm{m_l}$	External load mass
$\mathrm{t_l}$	External load torque
τ_w	Wheels torque
f_m	Lift force
τ_a	Arm torque

A. Kinematics

The direct kinematics of the robot can be expressed using equations (1) and (2), which represent the pose of the end effector and the coordinates of the CoG, respectively. Where $s_\circ$ and $c_\circ$ represent $sin(\theta_\circ)$ and $cos(\theta_\circ)$.

$$H_T^B = \begin{pmatrix} 1 & 0 & 0 & s_p(\mathrm{l_h}+d_m)+\mathrm{l_a} \\ 0 & 1 & 0 & 0 \\ 0 & 0 & 1 & r_w + c_p(\mathrm{l_h}+d_m) \\ 0 & 0 & 0 & 1 \end{pmatrix} \tag{1}$$

$$CoG = \begin{pmatrix} \frac{\mathrm{m_l}\left(d_m s_p + \mathrm{l_h} s_p + \frac{\mathrm{t_l}}{g\,\mathrm{m_l}}\right) + \mathrm{m_a}(\mathrm{l_a}+d_m s_p+\mathrm{l_h} s_p) + \mathrm{m_b}(\mathrm{l_{bz}} s_p - \mathrm{l_{bx}} c_p) + \mathrm{m_m}(d_m+\mathrm{l_m}) s_p}{\mathrm{m_a}+\mathrm{m_b}+\mathrm{m_l}+\mathrm{m_m}} \\ \frac{(\mathrm{m_a}+\mathrm{m_l})(d_m c_p + \mathrm{l_h} c_p) + \mathrm{m_b}(\mathrm{l_{bz}} c_p + \mathrm{l_{bx}} s_p) + \mathrm{m_m}(d_m+\mathrm{l_m}) c_p}{\mathrm{m_a}+\mathrm{m_b}+\mathrm{m_l}+\mathrm{m_m}} \end{pmatrix} \tag{2}$$

The terms $\mathrm{m_l}$ and $\mathrm{t_l}$ correspond to the estimated mass and generated torque of the load placed over the fork, respectively. To achieve the desired behavior of the system, the Z position of the end effector and the X coordinate of the CoG are the expressions of interest to manipulate the load and obtain a desired trajectory profile. Additionally, to use trajectory profiles for the end effector along the Z direction, it is important to consider the differential kinematics of the robot.

B. Dynamics

Equation (3) represents the solution of the Euler-Lagrange equation for the TWFR.

$$
\begin{aligned}
&M(q)\ddot{q} + H(\dot{q}, q) + G(q) = \tau \\
&q = [\theta_w \quad \theta_p \quad d_m \quad \theta_a]^T \\
&\tau = [n_w\tau_w \quad -n_w\tau_w \quad f_m \quad n_a\tau_a]^T \\
&M = \begin{pmatrix} m11 & m12 & m13 & m14 \\ m21 & m22 & m23 & m24 \\ m31 & m32 & m33 & m34 \\ m41 & m42 & m43 & m44 \end{pmatrix} \\
&H = \begin{pmatrix} h1 \\ h2 \\ h3 \\ h4 \end{pmatrix} \quad G = \begin{pmatrix} 0 \\ g2 \\ g3 \\ g4 \end{pmatrix}
\end{aligned} \tag{3}
$$

The above-presented expression is used in the following section to formulate the different control strategies. Nevertheless, an alternative representation of the system is used to define trajectory profiles for the robot. Fig. 3 illustrates a simplified model of the TWFR where the robot is modeled as a single-link inverted pendulum with mass $m_t = m_b + m_m + m_a + m_l$, angle $\theta_t = atan(\frac{CoG_x}{CoG_z})$, and length $\mathrm{l_t} = \|CoG\|$.

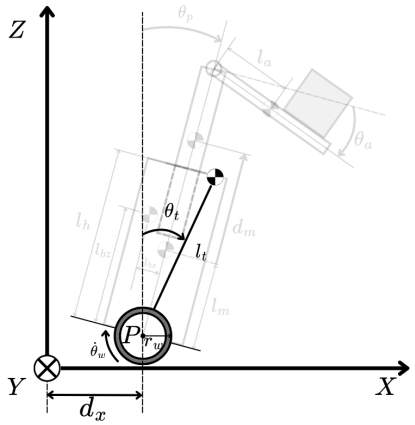

Fig. 3: Simplified model of the TWFR.

The solution of the Euler-Lagrange equation for the simplified system is presented in equation (4). With this simplified system, it is possible to establish a correlation between the angle θ_t and the desired horizontal acceleration of the robot $\ddot{x}$.

$$
\begin{aligned}
&M^*(q')\ddot{q'} + H^*(\dot{q'}, q') + G^*(q') = \tau^*(\ddot{x}) \\
&q' = [\theta_w \quad \theta_t]^T \\
&\tau^*(\ddot{x}) = [n_w\tau_w(\ddot{x}) \quad -n_w\tau_w(\ddot{x})]^T \\
&M^* = \begin{pmatrix} m11 & m12 \\ m21 & m22 \end{pmatrix} \\
&H^* = \begin{pmatrix} h1 \\ 0 \end{pmatrix} \quad G^* = \begin{pmatrix} 0 \\ g2 \end{pmatrix}
\end{aligned} \tag{4}
$$

On the other hand, the kinematic expressions (5) establish the relation between the simplified and complete model of the robot.

$$
\begin{cases}
r_w + c_p(\mathrm{l_h} + d_m) = z \\
c_p\dot{d}_m - s_p(\mathrm{l_h} + d_m)\dot{\theta}_p = \dot{z} \\
CoG_x(\theta_p, d_m, \mathrm{m_l}, \mathrm{t_l}) = sin(\theta_t)l_t \\
\dot{\theta}_p = 0
\end{cases} \tag{5}
$$

The solution of the system of equations that includes (4) and (5) for $\theta_p, \dot{\theta}_p, d_m, \dot{d}_m$ provides the reference values for the joints that allow the TWFR to track trajectory references along the Z and X axes simultaneously.

IV. Control

The low-level control of the robot is achieved using different disturbance observers and controllers for each subsystem.

A. Synthesized Pitch Angle Disturbance Observer (SPADO)

SPADO is used to model the unified disturbances that affect the angle of the wheels and the pitch angle of the robot due to the underactuated condition of the system. Equations (6), (7), and (8) present the procedure to find the total disturbance over the wheel's angle caused by interference torques of the other subsystems, modeling errors, and external torques.

$$
m_{11}\ddot{\theta}_w + m_{12}\ddot{\theta}_p + m_{13}\ddot{d}_m + m_{14}\ddot{\theta}_a + h_1 = n_w\tau_w - T_{lw} \tag{6}
$$

$$
m_{n11}\ddot{\theta}_w^{res} = n_w\tau_w^{ref} - \widetilde{\tau}_w^{dist} \tag{7}
$$

$$
\begin{aligned}
\widetilde{\tau}_w^{dist} = &(m_{11} - m_{n11})\ddot{\theta}_w + m_{12}\ddot{\theta}_p \\
&+ m_{13}\ddot{d}_m + m_{14}\ddot{\theta}_a + h_1 + T_{lw}
\end{aligned} \tag{8}
$$

Equations (9), (10), and (11) present the procedure to find the total disturbance over the pitch angle caused by interference torques of the other subsystems, modeling errors, and external torques.

$$
\begin{aligned}
&m_{21}\ddot{\theta}_w + m_{22}\ddot{\theta}_p + m_{23}\ddot{d}_m + m_{24}\ddot{\theta}_a \\
&\qquad + h_2 + g_2 = -n_w\tau_w - T_{lp}
\end{aligned} \tag{9}
$$

$$
m_{n21}\ddot{\theta}_w^{res} + m_{n22}\ddot{\theta}_p^{res} = -n_w\tau_w^{ref} - \widetilde{\tau}_p^{dist} \tag{10}
$$

$$
\begin{aligned}
\widetilde{\tau}_p^{dist} = &(m_{21} - m_{n21})\ddot{\theta}_w + (m_{22} - m_{n22})\ddot{\theta}_p \\
&+ m_{23}\ddot{d}_m + m_{24}\ddot{\theta}_a + h_2 + g_2 + T_{lp}
\end{aligned} \tag{11}
$$

Equation (12) is obtained by substituting (7) in (10).

$$m_{n22}\ddot{\theta}_p^{res} + \frac{m_{n21}+m_{n11}}{m_{n11}} n_w \tau_w^{ref} = \frac{m_{n21}}{m_{n11}} \widetilde{\tau}_w^{dis} - \widetilde{\tau}_p^{dist} \quad (12)$$

Finally, the synthesized disturbance is expressed by equation (13)

$$\widetilde{\tau}_s^{dist} = \widetilde{\tau}_p^{dist} - \frac{m_{n21}}{m_{n11}} \widetilde{\tau}_w^{dis} \quad (13)$$

Equation (14) expresses the synthesized disturbance as a function of the pitch angle acceleration and the torque of the wheels, by using pseudo-differentiation over $\dot{\theta}_p^{res}$. Equation (15) estimates the disturbance that will be used for the torque reference.

$$m_{n22}\ddot{\theta}_p^{res} + \frac{m_{n21}+m_{n11}}{m_{n11}} n_w \tau_w^{ref} = -\widetilde{\tau}_s^{dist} \quad (14)$$

$$\hat{\tau}_s^{dist} = \frac{g_s}{s+g_s}\left(g_s m_{n22}\dot{\theta}_p^{res} - \frac{m_{n21}+m_{n11}}{m_{n11}} n_w \tau_w^{ref} \right) - g_s m_{n22}\dot{\theta}_p^{res} \quad (15)$$

B. Pitch Angle Control

The vertical stabilization of the robot is accomplished by a PD controller implemented for the robot's pitch angle. The reference torque is determined using the candidate Lyapunov function (16) to guarantee a convergent behavior for the pitch angle. With equations (17) and (18), it is possible to find an expression for $\ddot{\theta}_p^{res}$ that is used in equation (14) to determine the reference torque for the pitch angle expressed in equation (19).

$$V = \frac{1}{2}K_1(\theta_p^{cmd} - \theta_p^{res})^2 + \frac{1}{2}K_2(\dot{\theta}_p^{cmd} - \dot{\theta}_p^{res})^2 \quad (16)$$

$$\dot{V} = (\dot{\theta}_p^{cmd} - \dot{\theta}_p^{res})\big(K_1(\theta_p^{cmd} - \theta_p^{res}) + K_2(\ddot{\theta}_p^{cmd} - \ddot{\theta}_p^{res})\big) \quad (17)$$

$$\dot{V} = -K_3(\dot{\theta}_p^{cmd} - \dot{\theta}_p^{res})^2 \quad (18)$$

$$\tau_w^{ref} = -\frac{m_{n11}m_{n22}}{n_w(m_{n21}+m_{n11})}\big(K_{pp}(\theta_p^{cmd} - \theta_p^{res}) + K_{dp}(\dot{\theta}_p^{cmd} - \dot{\theta}_p^{res}) + \ddot{\theta}_p^{cmd}\big) - \frac{m_{n11}}{n_w(m_{n21}+m_{n11})}\hat{\tau}_s^{dist} \quad (19)$$

$$K_{pp} = \frac{K_1}{K_2}, \quad K_{dp} = \frac{K_3}{K_2} \quad (20)$$

C. Fork Disturbance Observer (FDOB)

Similarly, as it was previously presented, equations (21), (22), and (23) present the procedure to find the total disturbance over the fork angle caused by interference torques of the other subsystems, modeling errors, and external torques.

$$m_{41}\ddot{\theta}_w + m_{42}\ddot{\theta}_p + m_{43}\ddot{d}_m + m_{44}\ddot{\theta}_a + h_4 + g_4 = n_a\tau_a - T_{la} \quad (21)$$

$$m_{n44}\ddot{\theta}_a^{res} = n_a\tau_a^{ref} - \widetilde{\tau}_a^{dist} \quad (22)$$

$$\widetilde{\tau}_a^{dist} = m_{41}\ddot{\theta}_w^{res} + m_{42}\ddot{\theta}_p^{res} + m_{43}\ddot{d}_m^{res} + (m_{44} - m_{n44})\ddot{\theta}_a^{res} + h_4 + g_4 + T_{la} \quad (23)$$

FDOB uses the pseudo-differentiation method over $\dot{\theta}_a^{res}$ to estimate the disturbance torque.

$$\hat{\tau}_a^{dist} = \frac{g_a}{s+g_a}(n_a\tau_a^{ref} + g_a m_{n44}\dot{\theta}_a^{res}) - g_a m_{n44}\dot{\theta}_a^{res} \quad (24)$$

D. Fork Angle Control

For the fork subsystem, a PD controller is implemented that also considers the estimated disturbance torque as it is presented in (25)

$$\tau_a^{ref} = K_{pa}(\theta_a^{cmd} - \theta_a^{res}) + K_{da}(\dot{\theta}_a^{cmd} - \dot{\theta}_a^{res}) + \hat{\tau}_a^{dist} \quad (25)$$

E. Fork Reaction Torque Observer (FRTOB)

By modeling the external load-dependent torque as (26), evaluating it in (23), and reorganizing the terms by making the disturbance torque independent of the effects of gravity and friction, the reaction torque of the fork due to an external load is obtained by (27).

$$T_{la} = \widetilde{\tau}_a^{ext} + \widetilde{\tau}_a^{fric} \quad (26)$$

$$\hat{\tau}_a^{reac} = \frac{g_r}{s+g_r}\big(n_a\tau_a^{ref} + g_r m_{n44}\dot{\theta}_a^{res} - g_4 - \widetilde{\tau}_a^{fric}\big) - g_r m_{n44}\dot{\theta}_a^{res} \quad (27)$$

This reaction torque is related to the term t_1 used in the kinematics equations as follows $t_1 = -\hat{\tau}_a^{reac}$

F. Lift Disturbance Observer (LDOB)

Analogously, as it was made for the fork subsystem, equations (28), (29), and (30) present the procedure to find the total disturbance over the lift displacement caused by interference forces of the other subsystems, modeling errors, and external forces.

$$m_{31}\ddot{\theta}_w + m_{32}\ddot{\theta}_p + m_{33}\ddot{d}_m + m_{34}\ddot{\theta}_a + h_3 + g_3 = f_m - F_{lm} \quad (28)$$

$$m_{n33}\ddot{d}_m^{res} = f_m^{ref} - \widetilde{f}_m^{dist} \quad (29)$$

$$\widetilde{f}_m^{dist} = m_{31}\ddot{\theta}_w^{res} + m_{32}\ddot{\theta}_p^{res} + (m_{33} - m_{n33})\ddot{d}_m^{res} + m_{34}\ddot{\theta}_a^{res} + h_3 + g_3 + F_{lm} \quad (30)$$

LDOB uses the pseudo-differentiation method over $\dot{d}_m^{res}$ to estimate the disturbance force.

$$\hat{f}_m^{dist} = \frac{g_m}{s+g_m}(f_m^{ref} + g_m m_{n33}\dot{d}_m^{res}) - g_m m_{n33}\dot{d}_m^{res} \quad (31)$$

G. Lift Displacement Control

Again, a PD controller is implemented that also considers the estimated disturbance force as it is presented in (32)

$$f_m^{ref} = K_{pm}(d_m^{cmd} - d_m^{res}) + K_{dm}(\dot{d}_m^{cmd} - \dot{d}_m^{res}) + \hat{f}_m^{dist} \quad (32)$$

H. Lift Reaction Force Observer (LRFOB)

By modeling the external load-dependent force as (33), evaluating it in (30), and reorganizing the terms by making the disturbance force independent of the effects of gravity and friction, the reaction force of the fork due to an external load is obtained by (34).

$$F_{lm} = \widetilde{f}_m^{ext} + \widetilde{f}_m^{fric} \tag{33}$$

$$\begin{aligned}\hat{f}_m^{reac} = \frac{g_r}{s+g_r}\big(f_m^{ref} + g_r m_{n33}\dot{d}_m^{res} \\ - g_3 - \widetilde{f}_m^{fric}\big) - g_r m_{n33}\dot{d}_m^{res}\end{aligned} \tag{34}$$

This reaction force is related to the term $\mathrm{m_l}$ used in the kinematics equations as follows $\mathrm{m_l} = \frac{\hat{f}_m^{reac}}{g\,cos(\theta_p)}$

I. Wheel Position Control

Finally, the position control of the wheels is determined by setting a reference command for the pitch angle of the robot; this reference command is determined by the following PD controller.

$$\theta_p^{cmd-PD} = K_{pw}(\theta_w^{cmd} - \theta_w^{res}) + K_{dw}(\dot{\theta}_w^{cmd} - \dot{\theta}_w^{res}) \tag{35}$$

Thus, the total pitch angle reference command is determined by the inverse solution and the PD controller.

$$\theta_p^{cmd} = \theta_p^{cmd-IS} + \theta_p^{cmd-PD} \tag{36}$$

V. Results

A simple sequence of actions was designed to evaluate the performance of the proposed control and trajectory generation method. The robot is carrying a load of 5kg placed over the fork at 0.37m from its rotational axis. The sequence starts with a preliminary position stabilization, which is required after the initial perturbation caused by the external load. When the desired initial position is reached, the fork will lift the load from the initial Z coordinate of 0.6025m to the final height set at 0.9m. Afterwards, the robot will move forward 3m following the designed trajectory. During the execution of this horizontal movement, the fork will go down to its initial height and then go up again at 0.9m. When the robot reaches the desired position, the fork will lower the load to 0.7m, and simultaneously, it will move backwards to the initial x coordinate, following the same trajectory profile previously used. Table II presents the experimental parameters used to describe the controllers, observers, and physical properties of the TWFR.

It is possible to see in Fig. 4 and Fig. 5 how the robot is capable of following the proposed position profile with a maximum transient state error of 14.7cm, which occurred because of the initial perturbation caused by the external load. The steady state position error reaches a maximum value of 1.7cm during the execution of the proposed trajectory.

An S-velocity profile was designed for the proposed horizontal trajectory to avoid possible oscillations during the execution of the movement. Fig. 6 exhibits the behavior of the

Table II: Experimental parameters

Parameter	Explanation	Value
K_{pp}	P-gain of pitch angle control	200
K_{pd}	D-gain of pitch angle control	50
K_{pa}	P-gain of arm position control	200
K_{da}	D-gain of arm position control	50
K_{pm}	P-gain of lift position control	200
K_{dm}	D-gain of lift position control	50
K_{pw}	P-gain of wheel position control	0.07
K_{dw}	D-gain of wheel position control	0.09
g_s (rad/s)	Cutoff angular frequency of SPADO	$2\pi6$
g_a (rad/s)	Cutoff angular frequency of arm FDOB	$2\pi5$
g_r (rad/s)	Cutoff angular frequency of FRTOB, LRFOB	$2\pi1$
g_m (rad/s)	Cutoff angular frequency of LDOB	$2\pi4$
N_w	Wheel gear ratio	11
N_a	Arm gear ratio	33
I_{wy} (kg m^2)	Wheel inertia	0.0052
I_{by} (kg m^2)	Body inertia	4.0590
I_{my} (kg m^2)	Lift inertia	0.0482
I_{ay} (kg m^2)	Arm inertia	0.0890
$\mathrm{l_{bz}}$ (m)	Body CoG z coordinate	0.3206
$\mathrm{l_{bx}}$ (m)	Body CoG x coordinate	0.0246
$\mathrm{l_m}$ (m)	Lift CoG distance	0.3975
$\mathrm{l_a}$ (m)	Arm CoG distance	0.2200
$\mathrm{m_w}$(kg)	Wheel mass	1.21
$\mathrm{m_b}$ (kg)	Body mass	64.1
$\mathrm{m_m}$ (kg)	Lift mass	21.5
$\mathrm{m_a}$ (kg)	Arm mass	3.5
$\mathrm{m_l}$ (kg)	Load mass	5

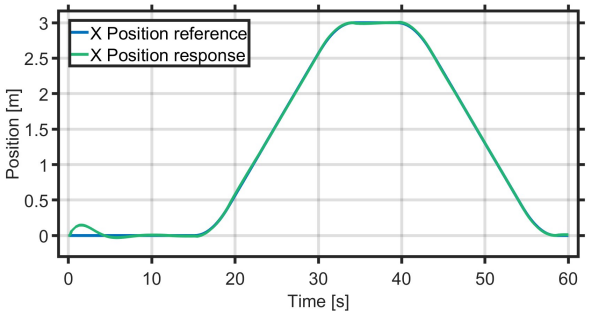

Fig. 4: Reference and response position of the TWFR along the X coordinate.

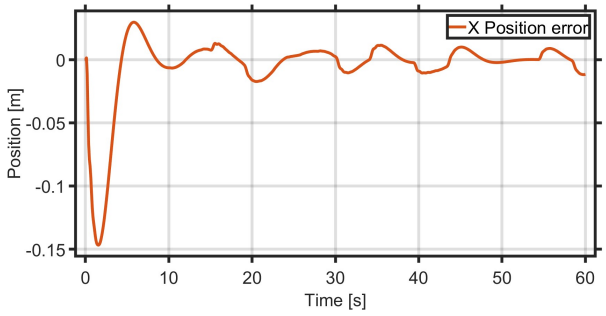

Fig. 5: Position error of the TWFR along the X coordinate during the execution of the proposed task.

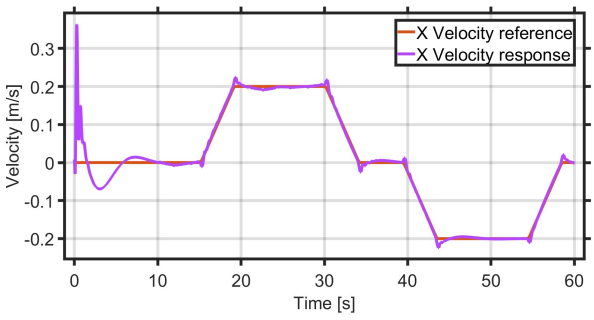

Fig. 6: Reference S-shape profile and response velocity of the TWFR along the X coordinate.

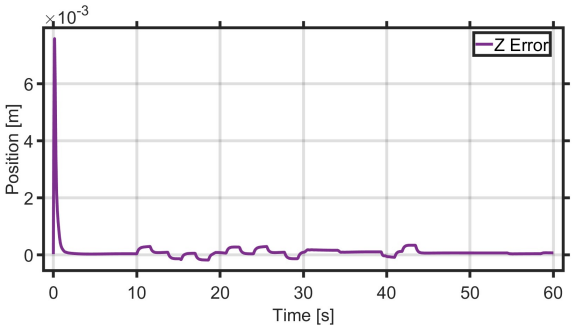

Fig. 7: Position error of the fork along the Z coordinate during the execution of the proposed task.

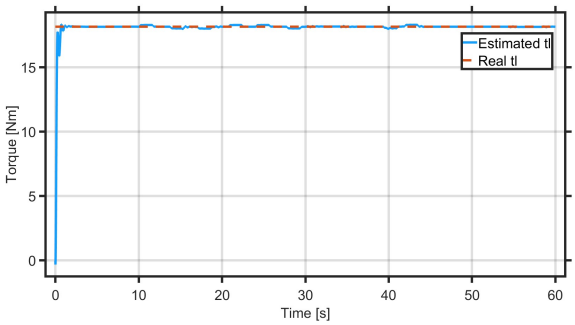

Fig. 8: Estimated value of the torque caused by the external load of 5kg placed at 0.37m from the rotational axis of the fork (18.142Nm).

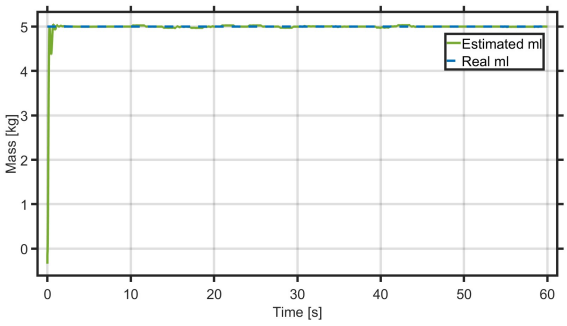

Fig. 9: Estimated value of the mass of the external load (5kg).

horizontal velocity of the system in contrast to the proposed reference. The velocity presents overshoots at the corners of the profile, which correspond with changes in the acceleration profile. On the other hand, the Z position of the fork follows the proposed trajectory with a maximum error of 7.58mm during the transient state and 0.3mm in the steady state, as depicted in Fig. 7.

Finally, the performance of the FRTOB and the LRFOB is evaluated in Fig. 8 and Fig. 9, respectively, estimating the value t_l and m_l that corresponds to the generated torque and the mass of the external load. It is possible to see how the dynamic behavior of both estimations is fast during the transient state and is almost a constant value during the steady state, which is beneficial for the IK and ID solutions that depend on these variables for the appropriate calculation of the motion profiles.

VI. Conclusions and Future work

As it was demonstrated throughout this work, the proposed motion planning and control strategies allow the TWFR to execute trajectories in the X and Z coordinate axes simultaneously with an admissible position error. The implementation of adaptive IK and ID solutions that depend on the estimation of physical properties of the external load provides great flexibility in industrial environments where it is not possible to control the variables of the load that will be manipulated. The next steps for this work are the construction of the lift subsystem and the physical implementation of the presented motion planning and control algorithms.

References

[1] H. Kanazawa, K. Ishizaki, Y. Miyata, M. Nawa, N. Kato, and T. Murakami, "Model-based pitch angle compensation for center of gravity variation in underactuated system with an arm," in *Proceedings of the 2023 IEEE 32nd International Symposium on Industrial Electronics (ISIE)*, 2023, pp. 1–6.

[2] J. Ito and T. Murakami, "Underactuated control for two-wheeled mobile robot with an arm using torque constraint conditions and disturbance observer," in *Proceedings of the 2023 IEEE 32nd International Symposium on Industrial Electronics (ISIE)*, 2023, pp. 1–6.

[3] H. Yajima, K. Ishizaki, Y. Miyata, M. Nawa, N. Kato, and T. Murakami, "Posture stabilization control compensating variation of body center of gravity in underactuated system," in *Proceedings of the 2023 IEEE International Conference on Mechatronics (ICM)*, 2023, pp. 1–6.